

# Resurgent Extrapolation: Rebuilding a Function from Asymptotic Data. Painlevé I

Ovidiu Costin<sup>1</sup> and Gerald V. Dunne<sup>2</sup>

<sup>1</sup> *Department of Mathematics, The Ohio State University, Columbus, OH 43210*

<sup>2</sup> *Department of Physics, University of Connecticut, Storrs, CT 06269*

Extrapolation is a generic problem in physics and mathematics: how to use asymptotic data in one parametric regime to learn about the behavior of a function in another parametric regime. For example: extending weak coupling expansions to strong coupling, or high temperature expansions to low temperature, or vice versa. Such extrapolations are particularly interesting in systems possessing dualities. Here we study numerical procedures for performing such an extrapolation, combining ideas from resurgent asymptotics with well-known techniques of Borel summation, Padé approximants and conformal mapping. We illustrate the method with the concrete example of the Painlevé I equation, which has applications in many branches of physics and mathematics. Starting solely with a finite number of coefficients from asymptotic data at infinity on the positive real line, we obtain a high precision extrapolation of the function throughout the complex plane, even across the phase transition into the pole region. The precision far exceeds that of state-of-the-art numerical integration methods along the real axis. The methods used are both elementary and general, not relying on Painlevé integrability properties, and so are applicable to a wide class of extrapolation problems.

## I. INTRODUCTION

Since exact solutions are rare in physics, asymptotic analysis is a common and powerful method for studying physical systems at extreme values of the relevant parameters, such as couplings, or masses, or temperature, or density, etc. For non-trivial physical systems, it is usually only possible to generate a *finite* number of terms in such an expansion. This raises the important question: how much information about the function being computed is encoded in this finite set of terms, generated in one particular asymptotic region? One class of such questions is the “central connection problem”: how can one extrapolate from strong coupling to weak coupling, or high temperature to low temperature, or high density to low density? This may enable access to the more difficult regime of *intermediate* values (neither small nor large) of coupling, or temperature, or density. Another class of questions involves extrapolation of the physical parameter from *real* values to *complex* values, or *vice versa*, a paradigm of which is the Lee-Yang-Fisher characterization of phase transitions in terms of complex zeros of the physical partition function [1, 2]. Motivated by these considerations, in this paper we study numerical methods to extrapolate finite-order perturbative expansions obtained in one parametric regime, at infinity in our chosen variable, down to zero and then throughout the entire complex plane. Extrapolation is of course a well-studied problem [3–7], and our new contribution is to demonstrate how and why ideas from resurgent asymptotics [8–14] significantly improve the numerical reach of such extrapolations. A subsequent paper [15] uses resurgent asymptotics to provide precise analytic estimates of the amount of information that can be extracted from a given number of terms, also based on the precision to which these terms are known. An intuitive explanation of why resurgence provides an advantage is that resurgent functions have an orderly structure in the Borel plane, which suggests that it may be possible to characterize or parametrize a resurgent function with a relatively small number of coefficients, if the extrapolation method is able to encode the resurgent structure in an efficient way. In this sense, our motivation also includes the possibility to extend conventional numerical algorithms to incorporate resurgent structure explicitly.

In this paper, we study the extrapolation of a particular concrete example, the Painlevé I equation. This choice is made for several reasons: (i) the Painlevé non-linear differential equations have many interesting applications in physics and mathematics [16–23], with the Painlevé I equation being of particular interest for matrix models and 2d quantum gravity [24–28]; (ii) the Painlevé I solutions have non-trivial analytic structure in the complex plane [29–44], which illustrates extrapolation from large to small parameter, and also Stokes phase transitions in the complex plane; (iii) the known analytic structure of Painlevé solutions permits high-precision diagnostic tests of the quality of our extrapolations. We stress that even though the Painlevé equations are of course very special, since they are integrable in the sense of Painlevé [45], the methods we use do not rely on this integrability. The class of resurgent problems is much larger than that of integrable problems, and indeed resurgence applies to all “natural problems” [9], for example those based on differential, or difference, or integral, equations, and so resurgent extrapolation methods are expected to have broad applicability in physics.

Section II explains how to generate our input “perturbative data” for the Painlevé I equation, and outlines the goals of our extrapolation. Section III reviews the well-known ideas of Borel summation, Padé approximants and conformal mapping applied to extrapolation along the real axis, as applied to Painlevé I. We show that conformal mapping

in the Borel plane significantly improves Padé-Borel extrapolation, and in Section IV we argue that this is because the conformal mapping reveals and encodes the underlying resurgent structure of the function being computed. In Section V we introduce a re-expansion method, based on Padé analysis in the physical plane, using our high-precision extrapolation along the real axis, which yields an extrapolation throughout the complex plane, crossing the phase transition into the *tritrionquée* pole region. Remarkably, only a modest amount of starting "perturbative data" is required in order to obtain non-trivial information about this phase transition and the structure of the pole region, which we confirm by comparing with known connection formulae and asymptotic estimates of pole locations.

## II. PAINLEVÉ I EQUATION: "PERTURBATIVE" ASYMPTOTIC INPUT DATA

The Painlevé I equation (referred to below as PI) in standard form reads [36, 38, 46]:

$$y''(x) = 6y^2(x) - x \quad (1)$$

Seeking a smooth real solution at large positive  $x$  leads to an asymptotic expansion of the form

$$y(x) \sim -\sqrt{\frac{x}{6}} \sum_{n=0}^{\infty} a_n \left( \frac{30}{(24x)^{5/4}} \right)^{2n}, \quad x \rightarrow +\infty \quad (2)$$

where  $a_0 \equiv 1$ , and with this choice of normalization all the expansion coefficients  $a_n$  are rational numbers [see (7)]. We define the natural "Écalle time" variable

$$t \equiv \frac{(24x)^{5/4}}{30} \quad (3)$$

It is convenient to extract the overall square root behavior and define the function  $h(t)$  by

$$y(x) \equiv -\sqrt{\frac{x}{6}} \left( 1 + h(t) \right) \quad (4)$$

In terms of  $h(t)$  the PI equation (1) becomes:

$$\ddot{h} + \frac{1}{t} \dot{h} + h \left( 1 + \frac{1}{2} h \right) - \frac{4}{25t^2} (1 + h) = 0 \quad (5)$$

where the overdot symbol denotes  $\frac{d}{dt}$ . The  $x \rightarrow +\infty$  asymptotic expansion (2) for  $y(x)$  becomes a  $t \rightarrow +\infty$  asymptotic expansion for  $h(t)$ :

$$h(t) \sim \sum_{n=1}^{\infty} \frac{a_n}{t^{2n}}, \quad t \rightarrow +\infty \quad (6)$$

where the  $a_n$  are the same numerical coefficients as in (2). Our strategy will be to analyze the function  $h(t)$ , and then use it to reconstruct the physical PI solution  $y(x)$  via the definitions (3)-(4).

The rational expansion coefficients  $a_n$  in (2) and (6) are generated from the recursion relation

$$a_n = -4(n-1)^2 a_{n-1} - \frac{1}{2} \sum_{m=2}^{n-2} a_m a_{n-m}, \quad n \geq 3$$

$$a_1 = \frac{4}{25}, \quad a_2 = -\frac{392}{625} \quad (7)$$

We take a certain number,  $N$ , of these coefficients as our input "perturbative data":

$$\begin{aligned} \text{perturbative input data} &= \{a_1, a_2, \dots, a_N\} \\ &= \left\{ \frac{4}{25}, -\frac{392}{625}, \frac{6272}{625}, -\frac{141196832}{390625}, \frac{9039055872}{390625}, \dots, a_N \right\} \end{aligned} \quad (8)$$

Our goal is to learn as much as possible about the function  $y(x)$ , starting solely from the perturbative input data (8). The Painlevé I equation (1) is used in our analysis to generate the input data [i.e., the coefficients  $a_n$  in (8)], and later as a diagnostic tool to test the level of precision of the resulting extrapolation.

We have the following specific technical goals:

1. Extrapolation of the formal "perturbative" expansion at  $x = +\infty$  in (2), starting with a *finite* number of terms, along the real axis all the way down to  $x = 0$ . This is the classical central connection problem for PI, for which there is no known closed-form solution. This is an analogue of determining strong-coupling behavior from weak-coupling asymptotics, or vice versa.
2. Extrapolation of the function  $y(x)$  into the complex  $x$  plane, once again starting just from the formal "perturbative" expansion at  $x = +\infty$  in (2), with a *finite* number of terms. At this stage, resurgent asymptotics begins to play a crucial role, both in terms of increased numerical precision, and also in terms of how much of the complex  $x$  plane can be explored accurately.
3. As a first step of the extrapolation into the complex plane, we show that the perturbative large  $x$  data in (8) permits a remarkably high-precision extraction of the PI Stokes constant, which is known analytically from isomonodromy methods [20, 34] and also from resurgent asymptotics [31, 32]. This enables probing of Stokes transitions, and access to higher Riemann sheets, purely from the asymptotic data on the positive real line. This is an analogue of determining non-perturbative effects from perturbative data.
4. Exploration of the transition into the PI pole region. It is well known that while the general solution to PI has poles throughout the complex  $x$  plane, distributed asymptotically according to those of an associated Weierstrass elliptic function [33–36], the formal expansion (2) defines Boutroux's *tr tronquée* solution to PI, which has poles in the complex  $x$  plane only in a wedge region of opening angle  $\frac{2\pi}{5}$  centered on the negative real  $x$  axis [38, 42]. We seek to explore this pole region numerically, mapping out its distribution and properties, once again starting just from the formal "perturbative" expansion at  $x = +\infty$  in (2), with a *finite* number of input coefficients. This is an analogue of probing a phase transition using perturbative expansion data generated from a point well away from the transition region. The behavior of the PI function  $y(x)$  changes radically as one crosses into the pole region, and its asymptotic trans-series expansion undergoes a dramatic rearrangement: the formal expansion (2) is completely different from the form of the function in the pole region: see Eq. (34). We seek to learn as much as possible about this transition from the finite perturbative input data in (8).

In our numerical extrapolation procedure we combine and compare several standard methods, such as Borel summation, Padé approximants and conformal mapping [3–7]. We incorporate ideas from resurgent asymptotics, with the goal of developing new extrapolation methods of increased precision and enlarged region of validity. Resurgence explains why conformal mapping is such a powerful step in this analysis. The resurgence of the Painlevé I equation is well established by general theorems and explicit computations [28–32, 40–43], and here our numerical analysis provides further numerical evidence of these features.

### III. EXTRAPOLATION ALONG THE REAL AXIS

In this Section we extrapolate the PI solution  $y(x)$ , starting with a finite number of terms in its formal asymptotic expansion (2) at  $x = +\infty$ , along the positive real axis down to  $x = 0$ , using various combinations of standard techniques, combined with some new improvements motivated by resurgent asymptotics. We compare the increased level of precision as the extrapolation method is refined. We perform our extrapolation directly on the formal asymptotic expansion (6) of the function  $h(t)$  defined in (4), and then map back to the physical PI solution  $y(x)$  using the definitions (2)–(4).

#### A. Borel Transform

The first observation is that the perturbative coefficients  $a_n$  in (2) and (6), generated from the recursion formula (7), alternate in sign and grow factorially fast in magnitude. The alternating sign property is directly correlated with the choice of overall sign in (2) [34, 36, 39]. With just 10 perturbative coefficients  $\{a_1, a_2, \dots, a_{10}\}$ , straightforward Richardson extrapolation [4] identifies the leading rate of growth as

$$a_n \sim (0.1967\dots)(-1)^{n+1}\Gamma\left(2n - \frac{1}{2}\right) + \dots, \quad n \rightarrow \infty \quad (9)$$

with the overall coefficient correct to 4 digits. Using 50 input coefficients permits a high-precision numerical identification of the overall coefficient, as well as extraction of subleading corrections:

$$a_n \sim \frac{1}{\pi} \sqrt{\frac{6}{5\pi}} (-1)^{n+1} \Gamma\left(2n - \frac{1}{2}\right) \left(1 - \frac{\frac{1}{8}}{(2n - \frac{3}{2})} + \frac{\frac{9}{128}}{(2n - \frac{3}{2})(2n - \frac{5}{2})} - \frac{\frac{341\,329}{1\,920\,000}}{(2n - \frac{3}{2})(2n - \frac{5}{2})(2n - \frac{7}{2})} + \dots\right), \quad n \rightarrow \infty \quad (10)$$

One can verify that the coefficients of the subleading corrections coincide with the low order coefficients of the expansion about the first exponential term in the trans-series expansion of the solution, as implied by general results of resurgent asymptotics [8–14, 47].

The factorial growth in (9)-(10) implies that the expansions (2) and (6) are formal divergent series, and therefore a natural next step is to define the Borel transform [4, 10] as the inverse Laplace transform of  $h(t)$ :

$$\text{Borel transform:} \quad \mathcal{B}[h](p) \equiv \sum_{n=1}^{\infty} \frac{a_n}{(2n-1)!} p^{2n-1} \quad (11)$$

The formal  $t \rightarrow +\infty$  series for  $h(t)$  in (6) is recovered by the Laplace transform:

$$\text{inverse Borel transform:} \quad h(t) \sim \int_0^{\infty} dp e^{-pt} \mathcal{B}[h](p) \quad (12)$$

Thus, the task of extrapolating and analytically continuing the function  $h(t)$  [and therefore also the Painlevé solution  $y(x)$ ] along the real axis, and into the complex plane, becomes the problem of understanding the singularity structure and analytic continuation of the Borel transform  $\mathcal{B}[h](p)$  in the complex  $p$ -plane, the Borel plane. The pragmatic question is:

How much can we learn about the Borel function  $\mathcal{B}[h](p)$  from just a *finite* number of perturbative coefficients of the small  $p$  expansion defined in (11)?

## B. Padé Analysis of the Borel Transform

The Borel transform series (11) has a finite radius of convergence, equal to 1, in the Borel  $p$  plane. This follows from the large-order growth in (9), and can also be seen from a simple ratio test [3]. It is also encoded in the distribution of poles of a Padé approximation to the Borel transform: see Fig. 1, which indicates singularities at  $p = \pm i$ . Given  $N$  coefficients in a truncated Borel transform

$$\text{truncated Borel transform:} \quad \mathcal{B}_N[h](p) \equiv \sum_{n=1}^N \frac{a_n}{(2n-1)!} p^{2n-1} \quad (13)$$

and noting that it is a polynomial of degree  $(2N-1)$ , we form the off-diagonal  $[N-1, N]$  Padé approximant [4, 48–50]

$$\text{Padé-Borel transform:} \quad \mathcal{PB}_N[h](p) = \frac{P_{N-1}(p)}{Q_N(p)} \quad (14)$$

where  $P_{N-1}(p)$  and  $Q_N(p)$  are polynomials of degree  $(N-1)$  and  $N$ , respectively. This Padé approximant step is completely algorithmic, and is indeed a built-in function in Mathematica and Maple. The Padé-Borel poles are shown in Fig. 1, for  $N = 10$ , and for  $N = 50$ . These poles are interlaced by the associated Padé zeros. Padé approximants represent a branch cut by a string of interlaced poles and zeros, so the Padé-Borel transform suggests the existence of branch cuts along the imaginary axes, with branch points at  $p = \pm i$ .

As a side-comment, we note that we have found that it is more numerically stable, especially when dealing with larger values of  $N$ , to convert the Padé approximant to its partial fraction decomposition:

$$\text{Partial fraction Padé-Borel transform:} \quad \mathcal{PB}_N[h](p) = \frac{P_{N-1}(p)}{Q_N(p)} = \sum_{k=1}^N \frac{r_k}{p - p_k} \quad (15)$$

where the sum is over the  $N$  Padé poles  $p_k$ , the zeros of  $Q_N(p)$ , with associated residues  $r_k$ . Since the Padé approximant is a rational function of  $p$ , the partial fraction expression in (15) is in principle equivalent to the Padé expression in

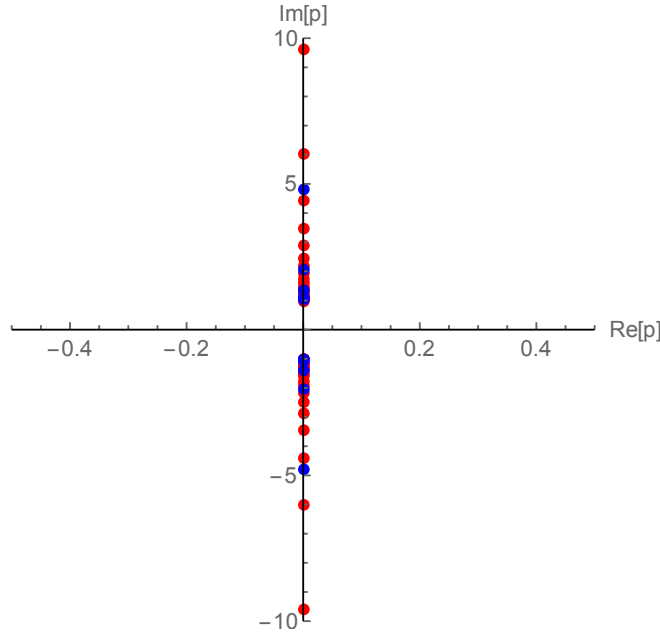


FIG. 1. Poles of the Padé approximation  $\mathcal{PB}_N[h](p)$  in (14) for the truncated Borel transform. The blue points are the Padé poles with  $N = 10$  input coefficients, and the red points represent the Padé poles with  $N = 50$  input coefficients. (Some further poles of  $\mathcal{PB}_{50}[h](p)$  are not shown, due to scale). Note that all the poles lie on the imaginary axis, and accumulate to branch points at  $p = \pm i$ .

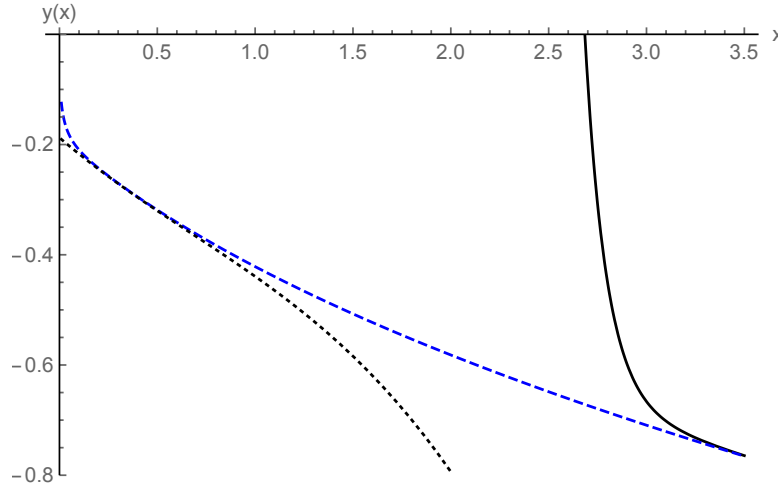


FIG. 2. A plot of the extrapolation of the PI function  $y(x)$ , from  $x = +\infty$  down to near  $x = 0$ , starting with just  $N = 10$  terms in (8) of the asymptotic expansion at  $x = +\infty$ . The solid black curve is based on (12) with the truncated Borel transform form  $\mathcal{B}_{10}[h](p)$  defined in (13), while the dashed blue curve is based on (12) with the Padé approximant  $\mathcal{PB}_{10}[h](p)$  defined in (14). The dotted black curve shows the first few terms of the Taylor expansion at  $x = 0$ , using the initial conditions for the PI *tritrinquée* solution from [36]:  $y(x) \approx -0.1875543083 - 0.3049055603x + 0.1055298557x^2 - 0.05229396374x^3$ . Note that the Padé-Borel transform extrapolates  $y(x)$  to much smaller values of  $x$  than does the 'raw' Borel transform. Starting with more input coefficients (i.e. larger values of  $N$ ), the improvement gets even better.

(14), but the increased numerical stability of (15) arises because the Padé expression at large order  $N$  tends to have very large coefficients in both numerator and denominator, thereby causing instabilities due to massive cancellations. In contrast, the residues and poles in the partial fraction expression (15) are much smaller in magnitude, and so the evaluation is more stable. This is a typical instability of Padé approximants. The resulting improved numerical stability of the partial fraction form can be important for subsequent numerical integrations over  $p$ , such as the Laplace transform integral in (12), required for returning to the original functions  $h(t)$  and  $y(x)$  in the physical  $t$  and  $x$  planes.

The Padé-Borel approximant in (14)-(15) is simple to compute, and it provides a significant extrapolation down the positive real line of the asymptotic expansion (2) of the PI solution  $y(x)$ . This is illustrated in Fig. 2, in which we plot the extrapolation obtained starting with  $N = 10$  terms. As a diagnostic comparison, we also plot [black dotted curve] the first four terms of the Taylor expansion of  $y(x)$  at the origin, using the initial conditions at the origin for the PI *tritrinquée* solution [36]:  $y(x) \approx -0.1875543083 - 0.3049055603x + 0.1055298557x^2 - 0.05229396374x^3 + \dots$ . Fig. 2 strongly suggests that the Padé-Borel extrapolation approaches the *tritrinquée* solution as  $x \rightarrow 0$ , while the "raw" Borel extrapolation begins to diverge from this behavior at  $x \approx 3$ . So, just 10 terms at  $x \rightarrow +\infty$  are required for the Padé-Borel extrapolation to extrapolate accurately down to  $x \approx 0.25$ . In the next Section we show that by combining the Padé-Borel method with conformal mapping we obtain a dramatic improvement on this already impressive precision of the Padé-Borel extrapolation.

Having determined the *location* of the leading singularities, the next step is to determine the *nature* of these singularities. There are several complementary ways to do this. A simple method is to use Darboux's theorem, which relates the nature of singularities to the large-order growth of coefficients of expansions about some other point [51, 52]. The large-order growth in (9) implies that the leading singularities at  $p = \pm i$  are square root singularities:

$$\mathcal{B}[h](p) \sim \frac{c}{\sqrt{p \mp i}} \quad , \quad p \rightarrow \pm i \quad (16)$$

for some constant  $c$ . This can also be extracted from the distribution of the interlacing Padé poles and zeros, but the Darboux analysis is simpler. Furthermore, invoking resurgence, the constant  $c$  in (16) is directly related to the Painlevé I Stokes constant:  $c = \frac{1}{2}S = \frac{1}{2\pi}\sqrt{\frac{3}{5}}$ . In Fig. 3 we plot the approach to the leading singularities, at  $p = \pm i$ , of the Padé-Borel approximation (14) to the Borel function, for  $N = 10$ . Fig. 3 displays rough numerical evidence for the approach to half the known Stokes constant for PI, marked as a horizontal dotted line. The Padé-Borel transform (14) is much better near the singularity than the raw Borel transform (13), but the behavior very close to the singularity still deviates from this resurgent expectation. With more input coefficients (larger  $N$ ) the curves approach closer to the Stokes value, but the deviation persists close to the singularity. This will be probed to significantly higher precision in the next Section, in which we introduce more powerful tools than just Padé-Borel. Compare, for example, with Fig. 7.

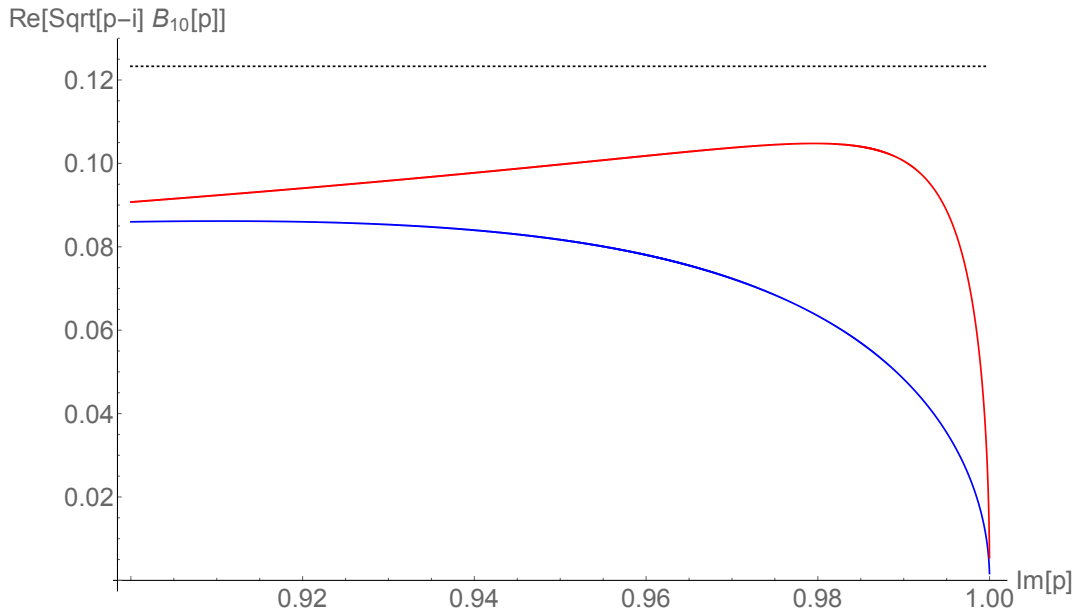


FIG. 3. An illustration of the square root branch cut behavior (16) of the Borel function as the leading singularity at  $p = +i$  is approached. The plot shows  $\text{Re}[\sqrt{p-i} \mathcal{B}_{10}[h](p)]$  based on the  $N = 10$  Borel transform (13) [blue curve], and based on the corresponding Padé-Borel transform (14) [red curve]. For reference, the dotted horizontal line is half the value of the Stokes constant,  $\frac{1}{2\pi}\sqrt{\frac{3}{5}}$ . This approach to the leading singularity is probed more precisely below, after the use of a suitable conformal map: see Figure 7.

### C. Conformal Mapping of the Borel Plane

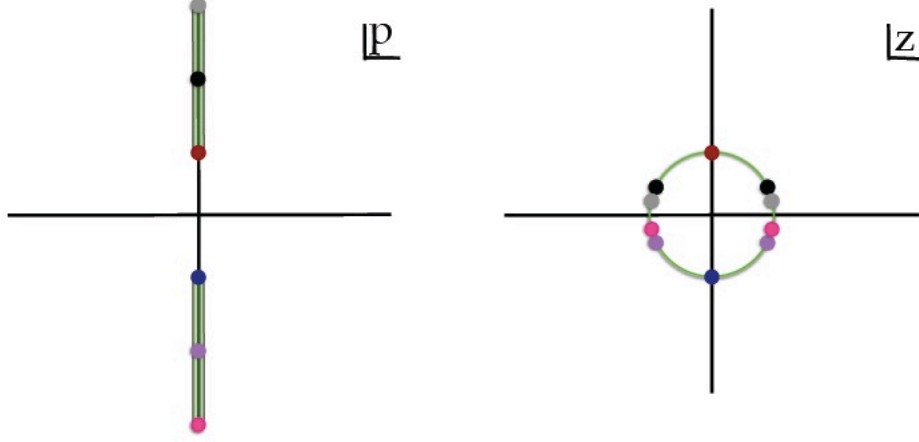


FIG. 4. The conformal map (17) from the doubly-cut Borel  $p$  plane [left] to the unit disc in the  $z$ -plane [right]. The cuts on the imaginary axis in the  $p$  plane are mapped to the unit circle in the  $z$  plane, marked by the green lines. The leading branch points at  $p = \pm i$  map to  $z = \pm i$ , marked by the red and blue dots. The resurgent second singularities at  $p = \pm 2i$ , on either side of the cuts, map to  $z = \pm e^{\pm i\pi/6}$ , marked by the black and purple dots, and the third singularities at  $p = \pm 3i$  map to  $\pm \frac{1}{3}(\sqrt{8} \pm i)$ , marked by the grey and pink dots.

To refine our numerical exploration of the properties of the Borel transform function  $\mathcal{B}[h](p)$ , we define a conformal map from the doubly-cut Borel  $p$  plane into the unit disc in the  $z$  plane:

$$\text{conformal map:} \quad z = \frac{p}{1 + \sqrt{1 + p^2}} \quad \longleftrightarrow \quad p = \frac{2z}{1 - z^2} \quad (17)$$

See Fig. 4. This maps the cuts along the imaginary axis in the Borel  $p$  plane to the unit circle in the complex  $z$  plane. The leading singularity at  $p = \pm i$  is mapped to  $z = \pm i$ . The resurgent second singularity at  $p = \pm 2i$ , on either side of the cut, is mapped to  $z = \pm e^{\pm i\pi/6}$ . Similarly, the resurgently repeated singularities at  $p_k \equiv \pm k i$ , map to points on the unit circle at  $z_k \equiv \pm \frac{1}{k}(\sqrt{k^2 - 1} \pm i k)$ , which approach  $z = \pm 1$  as  $k \rightarrow \infty$ . Thus the point at infinity in the  $p$  plane maps to  $z = \pm 1$ . Conformal mapping combined with Borel transforms is a well-known technique in physical applications [5–7, 53, 54], and here we quantify its improvement over the Padé-Borel transform discussed in the previous section, and we also use resurgent asymptotics to explain why such a significant improvement occurs.

We define a Padé-Conformal-Borel transform by the following algorithmic steps:

1. For a given number  $N$  of input coefficients, we evaluate the truncated Borel transform  $\mathcal{B}_N[h](p)$  in (13) at the conformally mapped location,  $p = \frac{2z}{1 - z^2}$ :

$$\text{Conformal-Borel transform:} \quad \mathcal{CB}_N[h](z) \equiv \mathcal{B}_N[h]\left(\frac{2z}{1 - z^2}\right) \quad (18)$$

By construction, this function is analytic inside the unit disc in the  $z$ -plane.

2. Re-expand  $\mathcal{CB}_N[h](z)$  about  $z = 0$  to the same order as the original Borel transform  $\mathcal{B}_N[h](p)$  in  $p$  [i.e., to  $O(z^{2N-1})$ ], and then construct a Padé approximant of the resulting truncated Taylor expansion, in the  $z$  plane:

$$\begin{aligned} \text{z-plane Padé-Conformal-Borel transform:} \\ \mathcal{PCB}_N[h](z) \equiv \text{Padé}_N \{ \text{Taylor expansion of } \mathcal{CB}_N[h](z) \} \end{aligned} \quad (19)$$

3. Invert the conformal map, evaluating the  $z$ -plane Padé approximant (19) at  $z = \frac{p}{1 + \sqrt{1 + p^2}}$ :

$$\begin{aligned} \text{p-plane Padé-Conformal-Borel transform:} \\ \mathcal{PCB}_N[h](p) \equiv \mathcal{PCB}_N[h]\left(z = \frac{p}{1 + \sqrt{1 + p^2}}\right) \end{aligned} \quad (20)$$

These steps of conformal mapping, followed by re-expansion and Padé approximation, and inverting the conformal map, yield our global approximation (20) to the Borel transform function in the original Borel  $p$  plane, which we call the “Padé-Conformal-Borel transform”. We stress that these steps are purely algorithmic, and furthermore they do not rely on any special integrability properties of the Painlevé I equation. In the next Sections we illustrate the numerical advantages of this conformal mapping procedure.

#### D. Increased Precision from the Padé-Conformal-Borel Transform

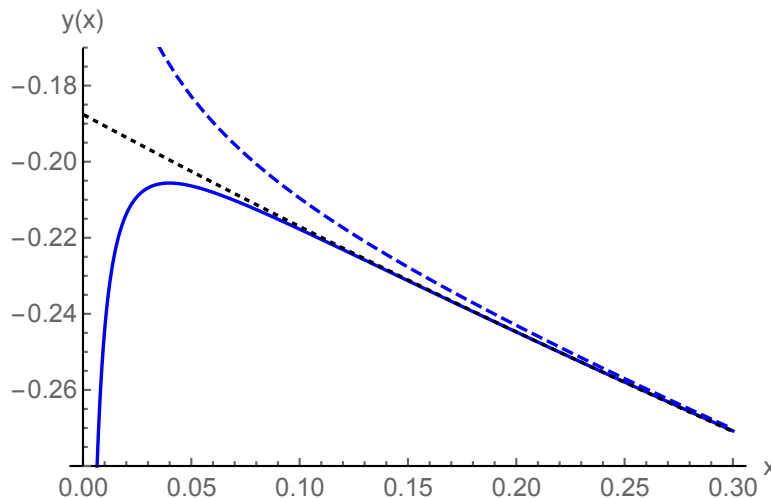


FIG. 5. The solid blue curve shows the PI function  $y(x)$  reconstructed from the Padé-Conformal-Borel transform  $\mathcal{PCB}_N[h](p)$  defined in (20), with  $N = 10$  input coefficients. For comparison, the dashed blue curve shows the result for  $y(x)$  from using the Padé-Borel transform  $\mathcal{PB}_{10}[h](p)$ , without the conformal mapping, as shown in Fig. 2. On this scale the original 10-term truncated Borel transform (13) (the solid black curve in Fig. 2) does not even appear. And as in Fig. 2, the dotted black curve shows the first few terms of the Taylor expansion at the origin, using the *tritrinquée* initial conditions. Note that both Borel transforms provide a remarkably good extrapolation from  $x = +\infty$  down to  $x \approx .25$ , with only 10 input coefficients in (8). However, with the same amount of input data, we see that the conformal-Padé-Borel extrapolation [solid blue curve] is significantly better at even smaller values of  $x$  than the Padé-Borel extrapolation [dashed blue curve]. See Fig. 6 for the analogous plot with  $N = 50$  input coefficients.

The first indication of higher precision using the Padé-Conformal-Borel transform, compared to the Padé-Borel transform, comes from performing the numerical inverse Borel transform integration in (12) to reconstruct the function  $h(t)$ , and hence the Painlevé I solution  $y(x)$  in the original  $x$  plane using (3)-(4). This leads to the numerical evaluation of an extrapolation of the PI solution  $y(x)$  along the positive  $x$  axis, using as input  $N$  terms of its asymptotic expansion (2) at  $x \rightarrow +\infty$ :

$$y_N(x) = -\sqrt{\frac{x}{6}} \left( 1 + \int_0^\infty dp \mathcal{B}_N[h](p) \exp \left[ -p \frac{(24x)^{5/4}}{30} \right] \right) \quad (21)$$

Here we can replace the Borel transform function  $\mathcal{B}_N[h](p)$  by either its Padé-Borel  $\mathcal{PB}_N[h](p)$  or Padé-Conformal-Borel  $\mathcal{PCB}_N[h](p)$  approximation, defined in (14) or (20) respectively. Figs. 5 and 6 compare the reconstructed function  $y_N(x)$  using the Padé-Borel transform [dashed curves], and using the Padé-Conformal-Borel transform [solid curves], for  $N = 10$  and  $N = 50$ , respectively. For reference, the dotted black line shows the (convergent) expansion of  $y(x)$  at the origin, using the approximate *tritrinquée* initial values [36]:  $y(0) \approx -0.1875543\dots$  and  $y'(0) \approx -0.34090556\dots$ . Figs. 5 and 6 show that *both* Borel transforms,  $\mathcal{PB}_N[h](p)$  and  $\mathcal{PCB}_N[h](p)$ , lead to remarkably precise extrapolations from  $x = +\infty$  down to very small values of  $x$ , even though the extrapolations are based on just 10 or 50 input coefficients from the asymptotic expansion at  $x = +\infty$ . However, we observe that in both cases the Padé-Conformal-Borel transform leads to a higher precision extrapolation at small  $x$ . In Section V we show how to obtain even better precision all the way to  $x = 0$ , and also into the negative  $x$  region and the complex  $x$  plane.



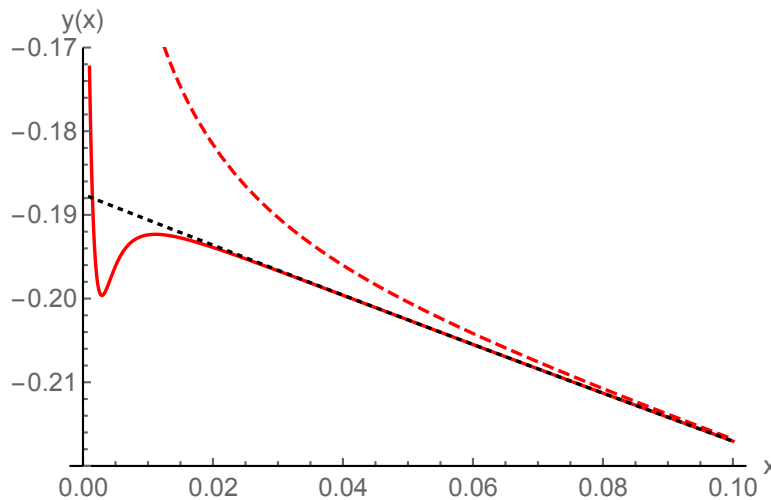


FIG. 6. As in Fig. 5, but now starting with  $N = 50$  perturbative input coefficients. The solid red curve shows the Padé-Conformal-Borel extrapolation of the PI function  $y(x)$ , starting from  $N = 50$  terms of the asymptotic large  $x$  expansion in (2), while the dashed red curve shows the extrapolation based on the Padé-Borel transform, without the conformal mapping. Once again, the conformal mapping extends the extrapolation to even smaller values of  $x$ . The black dotted curve shows the first few terms of the Taylor expansion of the PI *tritronquée* solution at the origin.

#### IV. EXTRAPOLATION INTO THE COMPLEX PLANE: RESURGENCE

In this Section we discuss how and why the Padé-Conformal-Borel transform  $\mathcal{PCB}_N[h](p)$  in (20) provides a much more precise representation of the true Borel transform function than the Padé-Borel transform  $\mathcal{PB}_N[h](p)$  in (14). The source of this improvement is the resurgent structure underlying the original asymptotic expansion, which is encoded more precisely by the Padé-Conformal-Borel transform. While the two Borel functions  $\mathcal{PCB}_N[h](p)$  and  $\mathcal{PB}_N[h](p)$  are very similar along the positive real  $p$  axis, important differences arise in the complex  $p$  plane, especially as one approaches the singularity lines on the imaginary  $p$  axis (see, for example, Figs. 10, 11, and 12, below). This affects the precision with which the contour of the Laplace transform in (21) can be deformed, thereby restricting the region of the complex  $x$  plane into which the Painlevé I function  $y(x)$  can be analytically continued with precision.

##### A. Precision Evaluation of the Painlevé I Stokes Constant

Invoking resurgence of the PI function  $y(x)$ , the behavior of the Borel transform function near its first singularities at  $p = \pm i$  determines the Painlevé I Stokes constant, and therefore governs the associated exponential corrections. This can be used as a precise numerical test of resurgence. Recall from Fig. 3 that the Padé-Borel function  $\mathcal{PB}_N[h](p)$  shows hints of the expected square root singularity behavior near the first singularity, but deviates as  $p$  approaches very close to  $\pm i$ . After conformal mapping, the Padé-Conformal-Borel transform is dramatically more precise in the vicinity of these first singularities, even with just  $N = 10$  input coefficients, as shown in Fig. 7. In fact, starting with just  $N = 10$  coefficients, the behavior of the Padé-Conformal-Borel transform near the leading singularity determines the Stokes constant to 4 digits of precision. And with  $N = 50$  digits we obtain 23 digits of precision. By contrast, probing the Padé-Borel transform near its first singularities allows just 1 digit of precision, at best. This is a dramatic improvement, which translates into a significant enlargement of the region of the complex plane in the physical variable  $x$  that can be accurately probed using the inverse Borel transform (21).

##### B. Resurgent Structure of Poles of the Padé-Conformal-Borel Transform

The underlying reason for the remarkable improvement of the Padé-Conformal-Borel transform is that the conformal map reveals the resurgent structure in the Borel plane, which is hidden in the pole structure of the Padé-Borel transform shown in Fig. 1. The conformal map separates and resolves the sub-structure of the Borel singularities, showing the repetition of singularities at integer multiples of the first singularities, as expected for a resurgent solution to a non-linear differential equation such as the Painlevé I equation (1) [9–14, 29–31].

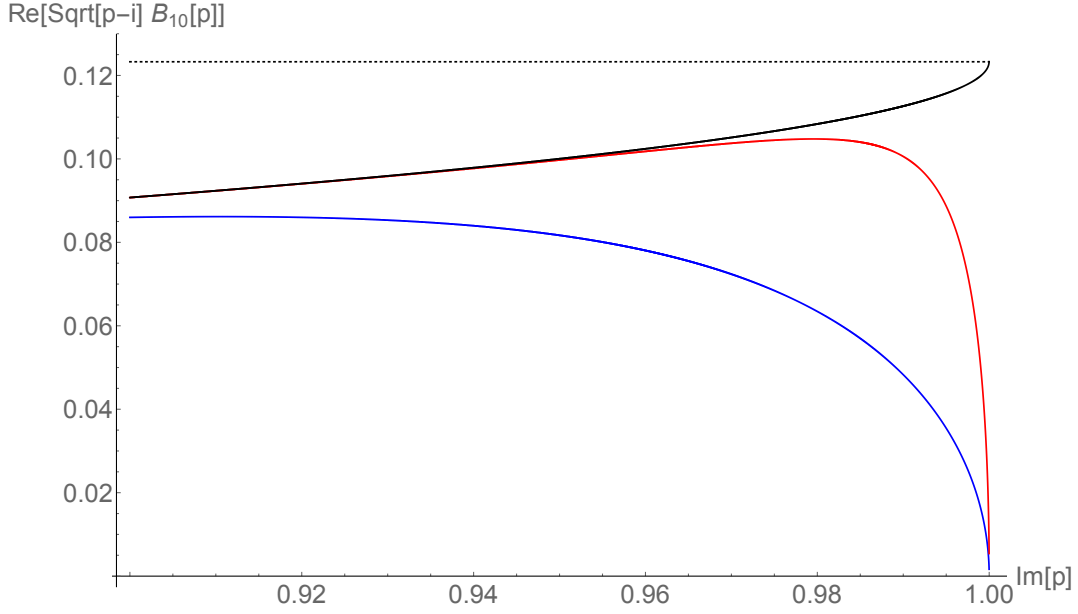


FIG. 7. An illustration of the square root branch cut behavior (16) of the Borel function as the leading singularity at  $p = +i$  is approached. The plot shows  $\text{Re}[\sqrt{(p-i)} \mathcal{B}_{10}[h](p)]$  based on the  $N = 10$  Borel transform [blue curve], Padé-Borel transform [red curve] and Padé-Conformal-Borel transform [black curve]. For reference the dotted horizontal line is half the value of the Stokes constant,  $\frac{1}{2\pi} \sqrt{\frac{3}{5}}$ .

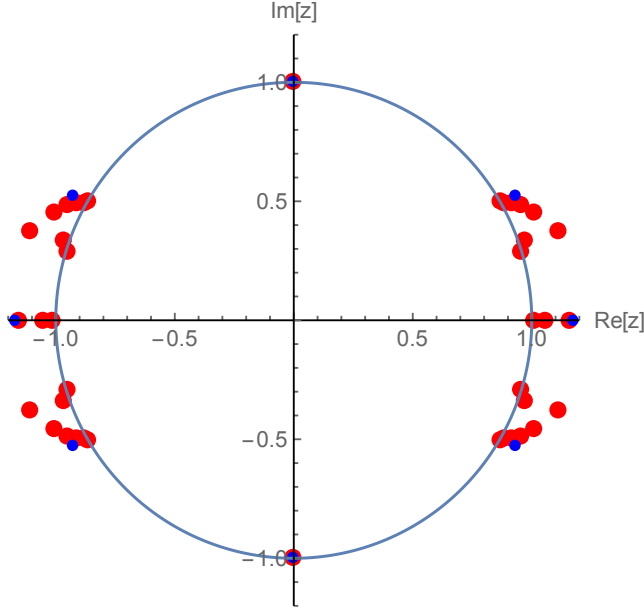


FIG. 8. Poles in the  $z$  plane of the conformally mapped Borel transform, for  $N = 10$  terms [blue] and 50 terms [red].

To see this, consider the poles in the conformally mapped  $z$  plane of the Padé-Conformal-Borel function  $\mathcal{PCB}_N[h](z)$  defined in (19). These are shown in Fig. 8, for  $N = 10$  and  $N = 50$ . These poles display the resurgent structure of the problem. The poles at  $z = \pm i$  are the conformal map images of the leading square root branch points at  $p = \pm i$  in the Borel  $p$  plane. Significantly, the conformal map has converted these branch cut singularities to simple poles, with residue proportional to the PI Stokes constant. Furthermore, these leading poles have been separated from the other singularities. This separation of the singularities according to their resurgent structure is a key factor in the improved precision of the subsequent numerical evaluations. Further observations concerning the  $z$  plane poles of the Padé-Conformal-Borel function  $\mathcal{PCB}_N[h](z)$  are:

1. There are no poles inside the unit disc in the  $z$  plane, since for any  $N$  the function  $\mathcal{PCB}_N[h](z)$  is analytic inside the unit disc, by construction<sup>1</sup>. The poles appear on or outside the boundary of the unit disc.
2. The poles on the *boundary* of the unit disc in the  $z$  plane are the conformal map images of  $p$  plane singularities on the cuts along the imaginary  $p$  axis.
3. The leading square-root singularities at  $p = \pm i$  have been conformally mapped to simple poles at  $z = \pm i$ , whose residue determines the Stokes constant  $S = \frac{1}{\pi} \sqrt{\frac{3}{5}}$  with remarkable precision. (Note that if the leading singularity were not of square root form, the conformal map would not map it to a pole; however, mapping to a pole can be achieved by suitable re-definition and convolution transformations. See the discussion in the Conclusions.)
4. The poles accumulating at  $z = \pm e^{\pm i \pi/6}$  are the conformal map images of singularities accumulating (from either side of the cuts) at  $p = \pm 2i$  in the  $p$  plane. We also see an indication of poles accumulating at  $z = \pm \frac{1}{3}(\sqrt{8} \pm i)$ , which are the conformal map images of singularities at  $p = \pm 3i$  in the  $p$  plane. With higher values of  $N$ , further  $p$  plane singularities at higher integer multiples of  $\pm i$  are resolved.
5. The poles outside the unit disc in the  $z$  plane correspond to information about the Borel transform on higher Riemann sheets, arising from analytic continuation across the  $p$  plane cuts. This information can be used for further numerical refinement.

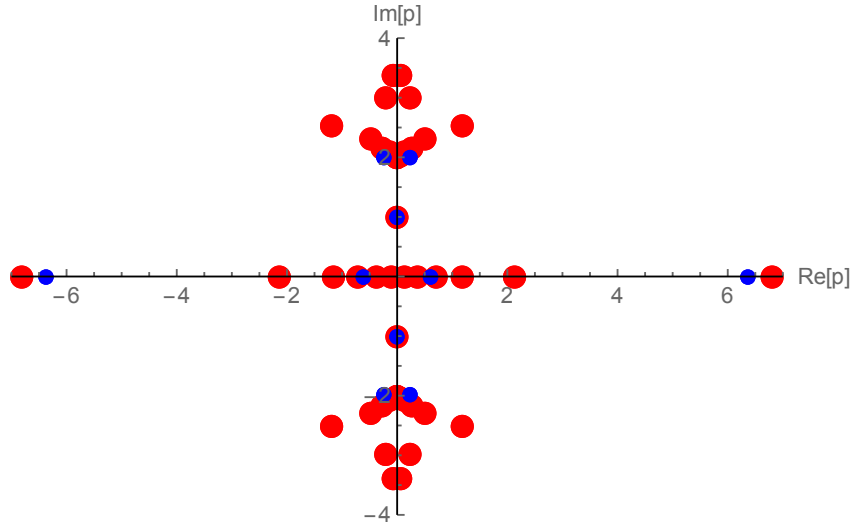


FIG. 9. The  $z$ -plane poles mapped back to the complex Borel  $p$  plane: 10 term expansion [blue], and 50 term expansion [red]. The leading singularity at  $p = \pm i$  is separated from the other singularities, and the next singularities accumulate at  $p = \pm 2i$ , the resurgently repeated next singularity, and with  $N = 50$  we see a hint of accumulation at the next singularity  $p = \pm 3i$ . The singularities on the real  $p$  axis, and off the imaginary  $p$  axis, are singularities on the next Riemann sheet.

This resurgent structure of singularities can also be seen in the Borel  $p$  plane. Fig. 9 shows the separation of the Borel singularities in the  $p$  plane after conformal mapping. Fig. 9 displays the inverse conformal maps of the  $z$  plane poles in Fig. 8. With  $N = 50$  terms [red dots] we see clearly the accumulation of singularities at  $p = \pm 2i$ , in addition to an indication of singularities at  $p = \pm 3i$ . It is straightforward to generate more perturbative input coefficients (i.e. larger  $N$ ), to reveal even higher singularities. Contrast this with Fig. 1, showing the poles of the Padé-Borel transform, before the conformal map, which shows no resurgent structure of repeated singularities.

This is not just a *qualitative* indication of the higher-order resurgent structure: the conformally mapped Borel transform also encodes *quantitative* information about the resurgent singularities. For example, comparing Figs. 3 and 7, we see that the coefficient of the leading singularity can be resolved by the Padé-Conformal-Borel function  $\mathcal{PCB}_{10}[h](p)$ , but not by the Padé-Borel function  $\mathcal{PB}_{10}[h](p)$ . Turning to the higher resurgent singularities, at integer

<sup>1</sup> In general, Padé may produce spurious poles, for example with anomalously small residues; these can be filtered if necessary [55], but we did not encounter this situation in this problem.

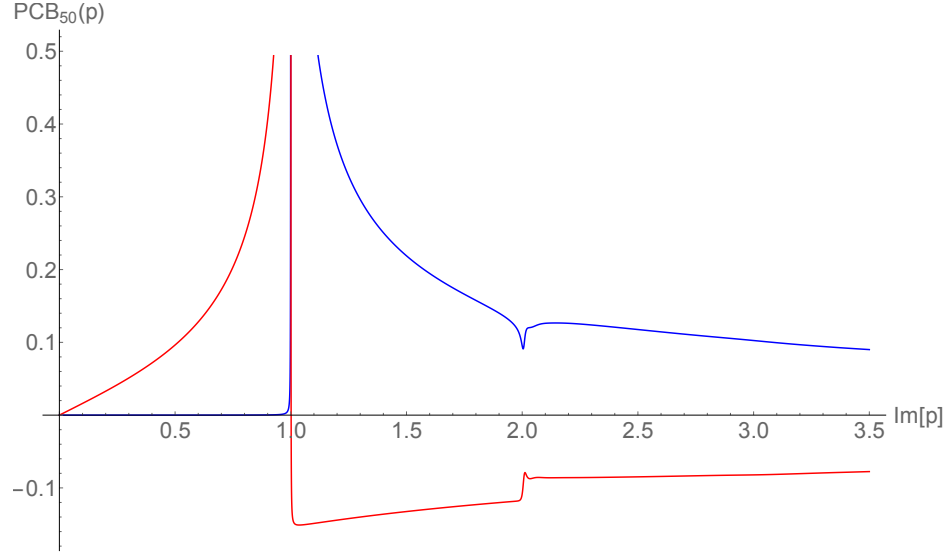


FIG. 10. A plot of the real [blue curve] and imaginary [red curve] parts of the conformally mapped Padé-Conformal-Borel transform  $\mathcal{PCB}_{50}[h](p)$ , defined in (20), along the imaginary  $p$  axis in the Borel  $p$  plane. We see clearly the first two singularities at  $p = +i$  and  $p = +2i$ , and an indication (after zooming in) of the third singularity at  $p = +3i$  (this, and higher singularities, can be further resolved with higher  $N$  values). A close-up view of the jump at  $p = +2i$  is shown in Fig 12.

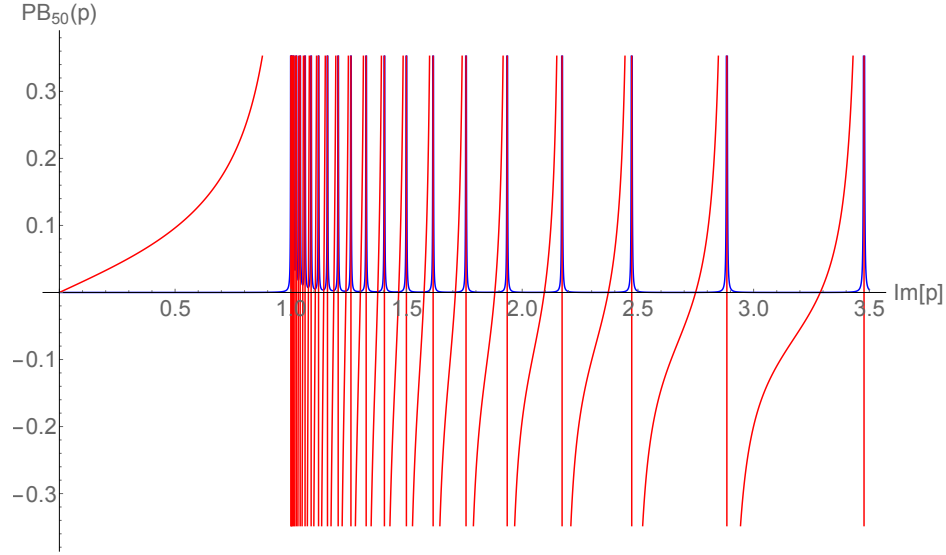


FIG. 11. A plot of the real [blue curve] and imaginary [red curve] parts of the Padé-Borel transform  $\mathcal{PB}_{50}[h](p)$ , defined in (14), along the imaginary  $p$  axis in the Borel  $p$  plane. Without the conformal map, none of the resurgent structure beyond the leading singularity can be resolved. Contrast with Fig. 10 and Fig. 12 for the conformally mapped Borel function, where the resurgent singularity at  $p = +2i$  is accurately resolved.

multiplies of  $\pm i$ , we contrast the behavior along the edge of the  $p$  plane cut shown in Fig. 10 [for the Padé-Conformal-Borel function  $\mathcal{PCB}_{50}[h](p)$ ] with that shown in Fig. 11 [for the Padé-Borel function  $\mathcal{PB}_{50}[h](p)$ ]. The Padé-Conformal-Borel function resolves the first two singularities (with a hint of the third when zoomed-in), while the Padé-Borel function does not resolve any of the higher resurgent singularities. Fig. 12 shows a close-up of the imaginary part of the Padé-Conformal-Borel function  $\mathcal{PCB}_N[h](p)$  along the imaginary  $p$  axis, in which we see clearly the resurgent jump at  $p = +2i$ . Furthermore, the *magnitude* of this jump coincides with that of the expected logarithmic behavior<sup>2</sup>

<sup>2</sup> The singularity is logarithmic because it is the inverse Laplace transform of the  $\left(\frac{e^{-t}}{\sqrt{t}}\right)^2$  term [29, 30].

at the second singularity:

$$\text{jump at second singularity} = \frac{1}{2}S^2 = \frac{1}{2} \left( \frac{1}{\pi} \sqrt{\frac{3}{5}} \right)^2 \approx 0.0304... \quad (22)$$

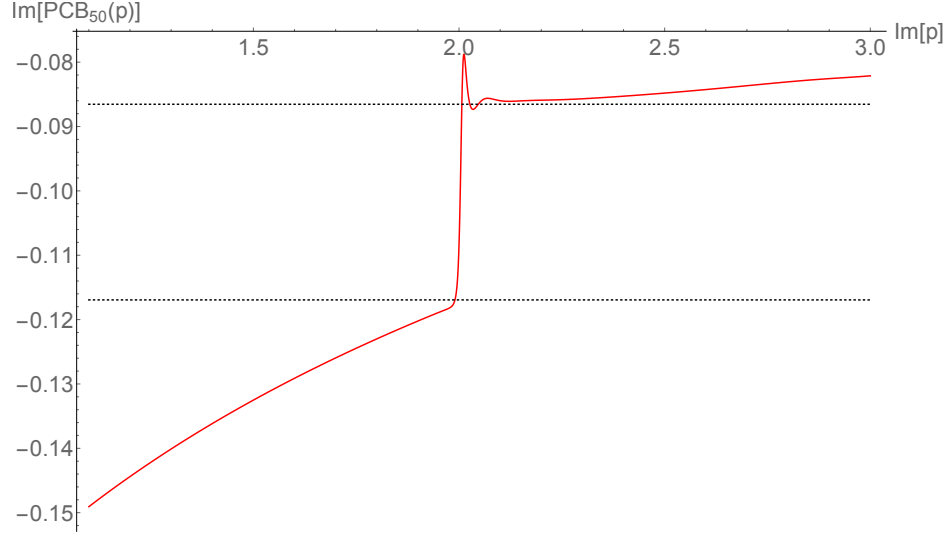


FIG. 12. Plot of the imaginary part of the Padé-Conformal-Borel transform  $\mathcal{PCB}_{50}[h](p)$  along the imaginary  $p$  line, zoomed-in from Fig. 10, showing the jump at the second singularity  $p = +2i$ . The dotted horizontal lines correspond to the resurgent jump associated with a logarithmic singularity, of magnitude  $\frac{1}{2}S^2$  as in Eq. (22).

## V. EXTRAPOLATION INTO THE PHYSICAL COMPLEX $x$ PLANE: THE ORIGIN AND THE POLE REGION

### A. Re-expansion Method and Precision Extrapolation to the Origin and Beyond

The fact that the Padé-Conformal-Borel transform  $\mathcal{PCB}_N[h](p)$  encodes the resurgent structure of the Borel transform, even along the most difficult directions along the cuts on the imaginary axis in the Borel  $p$  plane, suggests that the Laplace transform in (21) should be able to extrapolate the physical PI function  $y(x)$  throughout a much larger region of the complex  $x$  plane than is possible with the Padé-Borel transform. In this Section we explore this complex extrapolation, first all the way down to  $x = 0$ , then onto the *negative* real  $x$  axis, and then into the full complex  $x$  plane. While this can be achieved by numerical contour integration, a much simpler and significantly more accurate method is the following two-step procedure.

1. Use the Padé-Conformal-Borel method to extrapolate from the asymptotic  $x \rightarrow +\infty$  expansion (2) down to some small value  $x = x_0$  on the positive real axis, at which point the PI equation is satisfied to very high precision. As an illustration, we choose  $x_0 = 3$ . We extrapolate the function  $h(t)$  from  $t = +\infty$  along the real  $t$  axis down to  $t_0 \equiv (24x_0)^{5/4}/30 \approx 7$ , and evaluate  $h(t_0)$  and  $\dot{h}(t_0)$  by straightforward numerical Borel integration:

$$h_N(t_0) = \int_0^\infty dp e^{-pt_0} \mathcal{PCB}_N[h](p) \quad (23)$$

$$\dot{h}_N(t_0) = \int_0^\infty dp (-p) e^{-pt_0} \mathcal{PCB}_N[h](p) \quad (24)$$

Using the relation (4) between  $h(t)$  and  $y(x)$ , this yields extremely precise values for both  $y(x_0)$  and  $y'(x_0)$ . This precision is quantified below.

2. Generate a Padé approximant of the PI solution  $y(x)$  in the physical  $x$  plane, expanded about  $x = x_0$ . This Padé approximant can be generated using the PI equation, expressing all higher derivatives  $y^{(n)}(x_0)$  in terms of  $y(x_0)$  and  $y'(x_0)$ , in much the same way as the original perturbative coefficients were generated by expanding about  $x = +\infty$ . This step is algorithmic, but requires as input extremely precise values of  $y(x_0)$  and  $y'(x_0)$ . But this is exactly what our first step of Padé-Conformal-Borel extrapolation has produced.

To quantify the precision of the first step, we measure how well the extrapolated function satisfies the PI equation. Analogous to (23)–(24), we compute  $\ddot{h}_N(t_0)$  as a numerical integral,  $\ddot{h}_N(t_0) = \int_0^\infty dp (-p)^2 e^{-pt_0} \mathcal{PCB}_N[h](p)$ , which yields a value for  $y''(x_0)$ . The precision at  $x_0$  is then measured by the degree to which the PI equation (1) is satisfied. For example, using the Padé-Conformal-Borel transform  $\mathcal{PCB}_N[h](p)$  to extrapolate down to  $x_0 = 3$ , starting with just  $N = 10$  terms of the asymptotic expansion at  $x = +\infty$ , we satisfy the PI equation at  $x = x_0$  to 12 decimal places, and with  $N = 50$  terms it is satisfied to 29 decimal places. Had we used instead the Padé-Borel transform function  $\mathcal{PB}_N[h](p)$ , we still obtain impressive precision: 10 decimal places for  $N = 10$ , and 22 decimal places for  $N = 50$ :

$$N = 10 \text{ terms with Padé-Conformal-Borel: } [y''(x) - 6y^2(x) + x]_{x=3} = O(10^{-13}) \quad (25)$$

$$N = 50 \text{ terms with Padé-Conformal-Borel: } [y''(x) - 6y^2(x) + x]_{x=3} = O(10^{-30}) \quad (26)$$

$$N = 10 \text{ terms with Padé-Borel: } [y''(x) - 6y^2(x) + x]_{x=3} = O(10^{-11}) \quad (27)$$

$$N = 50 \text{ terms with Padé-Borel: } [y''(x) - 6y^2(x) + x]_{x=3} = O(10^{-23}) \quad (28)$$

The precision increases as  $\sqrt{N}$ , in agreement with analytic estimates [15].

This  $x$  space Padé approximation provides a simple analytic continuation of  $y_N(x)$  into the complex plane. For example, we can evaluate  $y_N(x)$  directly at the origin. We thereby obtain very precise values for the *tritronquée* initial conditions at the origin. With  $N = 10$  terms and Padé-Conformal-Borel input we obtain

$$\begin{aligned} N = 10 \text{ terms with Padé-Conformal-Borel:} \\ y(0) &\approx -0.187554308... \\ y'(0) &\approx -0.304905560... \\ y''(0) &\approx 0.211059715... \\ [y''(x) - 6y^2(x) + x]_{x=0} &= O(10^{-9}) \end{aligned} \quad (29)$$

and the PI equation is satisfied to 8 digit precision at the origin. With  $N = 50$  terms and Padé-Conformal-Borel input we obtain

$$\begin{aligned} N = 50 \text{ terms with Padé-Conformal-Borel:} \\ y(0) &\approx -0.18755430834049489383868175759583299323116090976213899693337265167... \\ y'(0) &\approx -0.30490556026122885653410412498848967640319991342112833650059344290... \\ y''(0) &\approx 0.21105971146248859499298968451861337073253247206264082468899143841... \\ [y''(x) - 6y^2(x) + x]_{x=0} &= O(10^{-65}) \end{aligned} \quad (30)$$

and the PI equation is satisfied to 64 digit precision at the origin. Padé-Borel input also leads to precise values at the origin, but with lower precision. This level of precision should be compared with roughly 14 digits of precision for  $y(0)$  and  $y'(0)$  obtained for Painlevé equations by the best current boundary-value, initial-value and Fredholm determinant numerical methods that operate along the positive real axis [56, 57]. The ultimate reason for the remarkable improvement in precision is that our extrapolation method incorporates the resurgent structure of the function, which encodes global information about the function throughout the entire complex plane, not just along the positive real axis.

As a further application, we can further continue the reconstructed function  $y_N(x)$  along the *negative* real  $x$  axis, where the PI *tritronquée* solution is known to have poles. Fig. 13 shows  $y_N(x)$  in this region, with  $N = 50$  input coefficients, with the first three (double) poles clearly visible. Even with  $N = 10$  input coefficients we accurately resolve the first pole on the negative  $x$  axis. The extrapolated function goes directly across the phase transition into this pole region, which we explore in further detail in the next section.

## B. Stokes Transition: Mapping the Tritronquée Pole Region

In this Section we cross the Stokes transitions in the physical  $x$  variable, at  $\arg(x) = \pm \frac{4\pi}{5}$ , and map the *tritronquée* complex pole region. The Dubrovin conjecture [38] states that for the *tritronquée* solution  $y(x)$  to PI, which has the

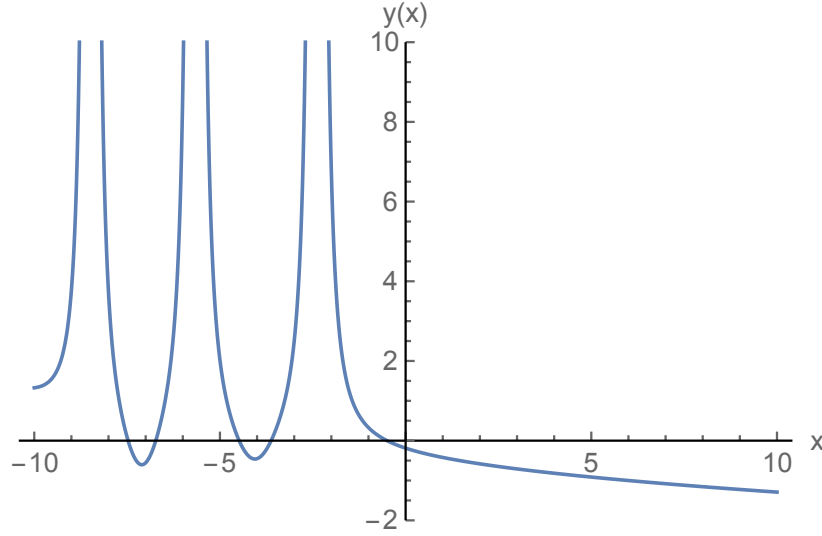


FIG. 13. Plot of the extrapolated function  $y(x)$  along the real  $x$  axis, showing the first three poles on the negative real axis. The function  $y(x)$  is obtained from  $N = 50$  input coefficients, and resolves accurately the first 3 poles on the negative real  $x$  axis.

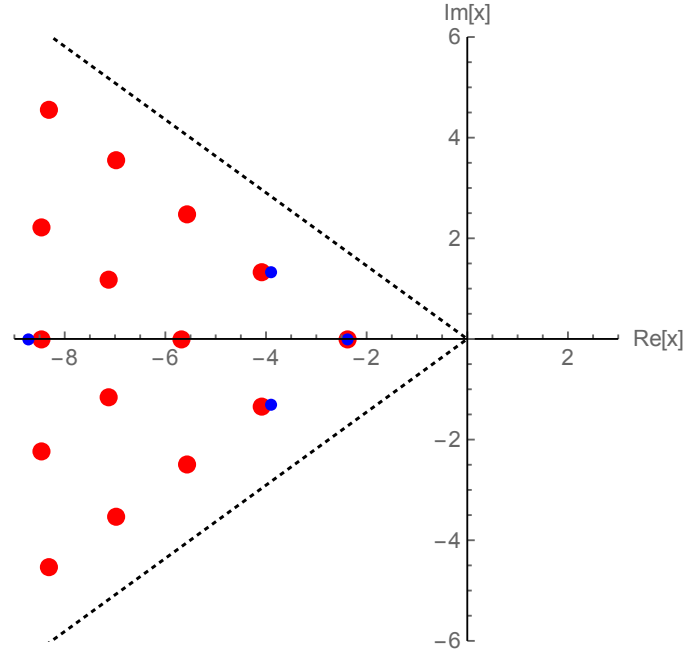


FIG. 14. Poles of our extrapolated PI solution  $y(x)$  in the complex plane. The smaller blue dots are extracted starting with just  $N = 10$  input coefficients (8) at  $x \rightarrow +\infty$ , while the larger red dots are extracted from  $N = 50$  input coefficients. The dashed lines mark the edges of the Stokes wedge for the *tritronquée* pole region:  $\frac{4\pi}{5} \leq \arg(x) \leq \frac{6\pi}{5}$ . This confirms the Dubrovin conjecture [38], stating that for the *tritronquée* PI solution the poles only lie within this wedge region.

asymptotic expansion (2) at  $x = +\infty$  [34–36], the only poles lie in the wedge region:  $4\pi/5 < \arg(x) < 6\pi/5$ . This conjecture has been proved in [42], and has been confirmed by several numerical analyses [39, 56, 57]. Here we use our resurgent extrapolation to give another high precision confirmation of this conjecture, combined with an analysis of the fine structure of the pole region.

Fig. 14 shows the poles of our analytically continued solution  $y_N(x)$ , obtained by combining the Padé-Conformal-Borel extrapolation with a Padé expansion at  $x_0 = 3$ , using just  $N = 10$  [blue dots], or  $N = 50$  [red dots], coefficients as input data. We stress that given the  $N$  input coefficients from (8), the rest of the computation is entirely algorithmic.

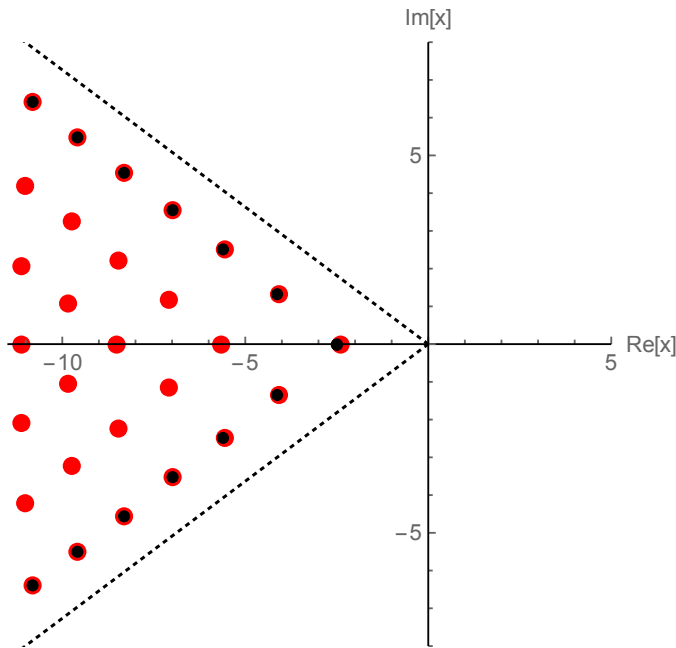


FIG. 15. The first 28 *tritronquée* poles,  $x_n$  [red dots] of the Painlevé I solution  $y(x)$ , obtained from our Padé-Conformal-Borel procedure, with  $N = 100$  input coefficients from (8), compared with the trans-asymptotic large  $n$  expression  $x_n^{\text{outer layer}}$  in (31) [smaller black dots]. The dashed lines mark the edges of the Stokes wedge for the *tritronquée* pole region:  $\frac{4\pi}{5} \leq \arg(x) \leq \frac{6\pi}{5}$ . Note that even at  $n = 1$ , the asymptotic large  $n$  expression (31) is surprisingly accurate.

We find it quite remarkable that with just 10 terms of the asymptotic expansion at  $x \rightarrow +\infty$ , the first three poles in the *tritronquée* pole region can be seen with reasonable precision. With 50 terms, we resolve the first 21 poles with a high degree of precision. It is a simple matter to work with even higher values of  $N$ , if further poles and/or higher precision are desired. See Fig. 15.

We see from Fig. 14 that the poles do indeed lie within the expected  $2\pi/5$  wedge, a numerical confirmation of the Dubrovin conjecture [38]. To probe the *tritronquée* poles more precisely, we compare them with the locations predicted by the trans-asymptotic analysis of [31, 32]. An asymptotic expression for the outer layer of poles in the *tritronquée* wedge is [31, 32]:

$$x_n^{\text{outer layer}} \approx e^{\frac{2\pi i}{5}} \left( \frac{30^{4/5}}{24} \right) \left( 2\pi i \left( n - \frac{1}{2} \right) + \ln \left( \frac{C}{12\sqrt{2\pi i n}} \right) - \dots \right)^{4/5}, \quad n \rightarrow \infty \quad (31)$$

and  $(x_n^{\text{outer layer}})^*$ , where  $C$  is proportional to the Stokes constant:  $C = i\sqrt{\frac{6}{5\pi}}$ . In Fig. 15 we compare the  $n \rightarrow \infty$  trans-asymptotic estimate in (31) with the numerical poles obtained from our Padé-Conformal-Borel procedure, starting with  $N = 100$  coefficients at  $x \rightarrow +\infty$ . The agreement with the  $n \rightarrow \infty$  asymptotics is remarkable, even all the way down to  $n = 1$  for the pole closest to the origin. Asymptotic formulas for successive layers of lines of poles can be derived straightforwardly from recursion relations for adiabatic invariants [31, 32].

We comment that in a very interesting paper [39], Novokshenov has made a Padé expansion of the PI solution  $y(x)$  directly at the origin in the physical  $x$  variable, which can be “tuned” to the *tritronquée* solution by adjusting the initial values  $y(0)$  and  $y'(0)$  according to the requirement that the resulting Padé approximant has no poles outside the *tritronquée* pole region wedge  $4\pi/5 < \arg(x) < 6\pi/5$ . To ensure that no poles leak outside of this region, this requires an extremely delicate search procedure, profoundly sensitive to the initial values  $y(0)$  and  $y'(0)$ ; and therefore a very efficient Padé algorithm was developed in [39]. By contrast, in our  $x$ -space Padé re-expansion method (see Sec. V A), the initial values  $y(0)$  and  $y'(0)$  are automatically fixed by our high-precision Padé-Conformal-Borel extrapolation, and no search is needed at all.

### C. Stokes Wedges and *Tritronquée* Connection Formulas

In this Section we plot our extrapolated PI solution  $y(x)$ , from Sec. V A, along the Stokes and anti-Stokes lines for the *tritronquée* solution. These are the most interesting and nontrivial directions in the complex  $x$  plane, describing the



transition boundaries between the five different Stokes wedges. Recall that the PI equation is invariant under rotation

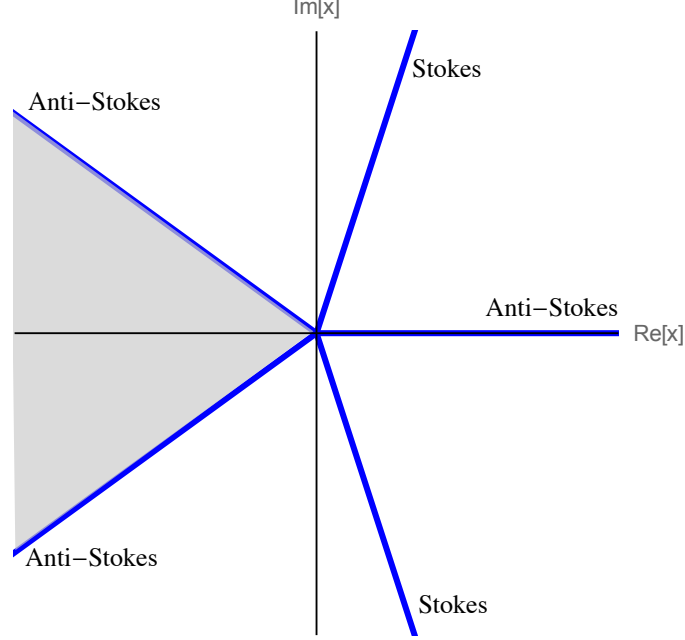


FIG. 16. The five Stokes wedges of the PI equation (1), showing the Stokes and anti-Stokes lines for the *tritronquée* solution, as lines with  $\arg(x) = k \frac{2\pi}{5}$ , with  $k = 0, \dots, 4$ . The shaded wedge is the *tritronquée* pole region:  $\frac{4\pi}{5} < \arg(x) < \frac{6\pi}{5}$ . Recall that our perturbative input (8), from which we have developed our extrapolation of the PI solution  $y(x)$  throughout the complex  $x$  plane, was obtained from the asymptotics as  $x \rightarrow +\infty$  along the anti-Stokes line on the positive real  $x$  axis.

of the coordinate  $x$  by  $e^{\frac{2\pi i}{5}}$ , and the function  $y$  by  $e^{\frac{4\pi i}{5}}$  [33–40], and the asymptotics (2) of the *tritronquée* solution defines the set of Stokes and anti-Stokes lines,  $\arg(x) = k \frac{2\pi}{5}$  with  $k = 0, \dots, 4$ , as shown in Fig. 16. Our perturbative input (8), from which we have developed our extrapolation of the PI solution  $y(x)$  throughout the complex  $x$  plane, was obtained from the large  $x$  asymptotics along one particular direction: the anti-Stokes line along the positive real axis. The behavior of  $y(x)$  along the other Stokes and anti-Stokes lines is very different. As a precise diagnostic check of the quality of our extrapolation into the complex  $x$  plane, we can test the known analytic connection formulas of the PI *tritronquée* solution, which relate the rotated *tritronquée* solutions along the Stokes and anti-Stokes lines [33–35, 40].

For example, the *tritronquée* solution  $y(x)$  along the positive  $x$  axis, and along the anti-Stokes line  $\arg(x) = \frac{4\pi}{5}$ , at the edge of the pole region, are related by the following exact connection formula, exhibiting oscillatory behavior with a coefficient depending on the Stokes constant [34, 35, 40]:

$$y(x) - e^{\frac{8\pi i}{5}} y\left(e^{\frac{4\pi i}{5}} x\right) \sim \frac{e^{-\frac{3\pi i}{4}}}{2^{5/4} 6^{1/8} \sqrt{\pi}} \frac{e^{-i(24x)^{5/4}/30}}{x^{1/8}}, \quad x \rightarrow \infty \quad (32)$$

Fig. 17 shows this combination using our extrapolated function  $y(x)$ , displaying the oscillatory behavior of (32), capturing accurately both the period and the amplitude. On the other hand, the *tritronquée* solution  $y(x)$  along the Stokes lines  $\arg(x) = \pm \frac{2\pi}{5}$  are related by the following exact connection formula, exhibiting exponentially decaying behavior, also with a coefficient depending on the Stokes constant [34, 35, 40]:

$$y(e^{-\frac{2\pi i}{5}} x) - e^{\frac{8\pi i}{5}} y\left(e^{\frac{2\pi i}{5}} x\right) \sim \frac{e^{-\frac{3\pi i}{4} + \frac{i\pi}{20}}}{2^{5/4} 6^{1/8} \sqrt{\pi}} \frac{e^{-(24x)^{5/4}/30}}{x^{1/8}}, \quad x \rightarrow \infty \quad (33)$$

Fig. 18 shows this combination using our extrapolated function  $y(x)$ , displaying the correct exponentially decaying behavior of (33).

#### D. Fine Structure of the Tritronquée Poles

The *general* PI solution  $y(x)$  is known to be meromorphic throughout the complex plane [19, 20, 33], and to have poles throughout the complex plane, in all five Stokes wedges. Indeed, in the vicinity of a moveable pole, the *general*

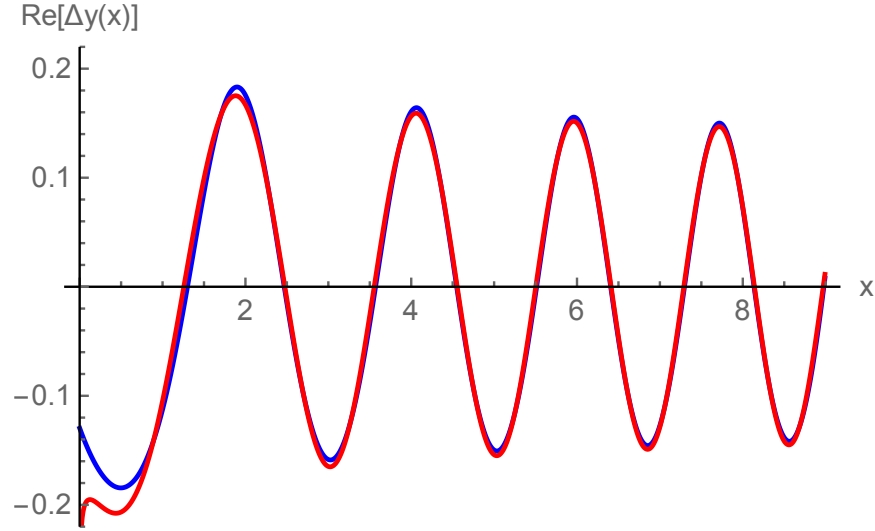


FIG. 17. Plot of the *tritronquée* connection formula (32). The blue curve is the real part of the left-hand-side of (32), while the red curve is the real part of the right-hand-side, using our Painlevé I solution  $y(x)$  extrapolated into the complex plane. Analogous plots can be made for the imaginary parts.

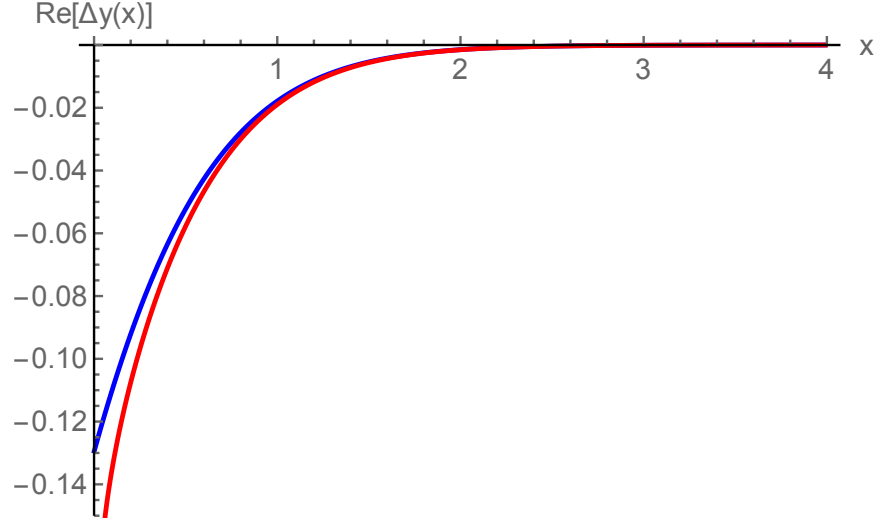


FIG. 18. Plot of the *tritronquée* connection formula (33). The blue curve is the real part of the left-hand-side of (32), while the red curve is the real part of the right-hand-side, using our Painlevé I solution  $y(x)$  extrapolated into the complex plane. Analogous plots can be made for the imaginary parts.

PI solution  $y(x)$  has a Laurent expansion of the following form

$$y(x) \approx \frac{1}{(x - x_{\text{pole}})^2} + \frac{x_{\text{pole}}}{10}(x - x_{\text{pole}})^2 + \frac{1}{6}(x - x_{\text{pole}})^3 + h_{\text{pole}}(x - x_{\text{pole}})^4 \\ + \frac{x_{\text{pole}}^2}{300}(x - x_{\text{pole}})^6 + \frac{x_{\text{pole}}}{150}(x - x_{\text{pole}})^7 + \dots \quad (34)$$

All further coefficients of this Laurent expansion are expressed as polynomials in the two parameters  $x_{\text{pole}}$  and  $h_{\text{pole}}$ . Thus, any PI solution  $y(x)$  is completely determined by two constants,  $x_{\text{pole}}$  and  $h_{\text{pole}}$ , *in the vicinity of any one of its poles*. The *tritronquée* is special in the sense that it has poles only in one Stokes wedge [38, 42] (see Sec. VB). Since our re-expansion method produces the most precise values for the pole closest to the origin, it is natural to use this first pole,  $x_1$  and its associated expansion constant  $h_1$ , to characterize the *tritronquée* solution to PI. In fact, since there is nothing special about  $x = 0$  for the PI equation, the data  $(x_1, h_1)$  is a much more natural way to characterize the *tritronquée* solution than giving  $y(0)$  and  $y'(0)$  at the origin. High precision values for the first pole and the



values is left for future work. This is motivated by results connecting poles of PI solutions to spectral properties of cubic oscillators [58–60], in analogy to results relating pole behavior of Painlevé III solutions with the spectrum of the Mathieu equation [61–63], and pole behavior of Painlevé VI solutions to spectral properties of an associated Heun equation [64, 65].

## VI. CONCLUSIONS

We have studied the numerical extrapolation of the solution  $y(x)$  to the Painlevé I equation (1), starting from a *finite* number of terms in the asymptotic expansion at  $x \rightarrow +\infty$ . Combining standard methods of Borel transforms, Padé approximants, and conformal mapping, together with aspects of resurgent asymptotics, we obtain a surprisingly precise extrapolation throughout the complex  $x$  plane. Our initial asymptotic expansion (2) generates the *tritrônquée* solution to PI, and we tested the precision of our extrapolation by comparing it with known analytic properties such as exact connection formulae and trans-asymptotic pole expressions. The extrapolated function crosses smoothly across the non-linear Stokes transitions into the pole region. Both Padé-Borel and the conformally mapped Padé-Conformal-Borel extrapolations produce high quality extrapolations, but the latter is more accurate in a larger range of the complex plane. The ultimate reason for this is that the conformal map resolves more efficiently the underlying regularity of the resurgent structure in the Borel plane. The resurgent extrapolation method is very general, not relying on the integrability of the Painlevé I equation, and should be applicable to the much broader class of resurgent problems in physics. Several extensions and refinements of the resurgent extrapolation method are possible, which may become more relevant in other problems where fewer perturbative coefficients can be generated, and/or if these coefficients are generated with limited precision. We list some of these refinements here, and further details will be given in subsequent papers.

*Duality Bootstrap:* the expansion of  $y(x)$  as  $x \rightarrow +\infty$  maps directly to the  $p \rightarrow 0$  behavior of the Borel transform, and correspondingly the behavior of  $y(x)$  as  $x \rightarrow 0$  maps directly to the  $p \rightarrow \infty$  behavior of the Borel transform. In certain cases the problem may be one of *interpolation*, in which some knowledge about both  $x \rightarrow +\infty$  and  $x \rightarrow 0$  is known, but one wants to interpolate between these two expansions in a way that accurately describes intermediate values of  $x$ . In this case, the duality between large and small  $x$ , and small and large  $p$  can be used to develop an iterative “bootstrap” procedure. In the case of PI, our extrapolation method already produced sufficient numerical precision, but in other problems this duality bootstrap can be a powerful additional tool.

*Singularity Tuning:* as mentioned in Sec. IV B, the leading Borel singularity for PI is of square root character [see (16)], and is mapped to a pole by the conformal map (17). In other problems, where the leading singularity is not a square-root branch point, one can apply ramified re-definitions of the expansion parameter and Borel variable in order to engineer a leading pole after conformal mapping. This facilitates the resurgent separation of the singularities, resulting in improved precision.

*Higher Riemann sheets:* we observed numerically that the Padé-Conformal-Borel produces singularities on higher Riemann sheets. These singularities could be used for further higher precision tests of resurgence, and also for a systematic numerical investigation of Écalle’s medianization [9, 11].

*Continued Fractions, Orthogonal Polynomials and Padé Approximants:* there is a deep connection between Padé, continued fractions, orthogonal polynomials and conformal mapping, which we discuss in detail in [15], but we comment briefly on the basic ideas here. The outcome of this connection is that one can derive analytic estimates of the precision that can be obtained by Padé-Borel and Padé-Conformal-Borel with  $N$  input coefficients. Resurgence appears in these extrapolations due to the fact that given  $N$  terms of an expansion, Padé can predict the next term with exponential precision. Analytic continued fractions [66], in one of the most useful normalizations, are rational functions of the form

$$R_N(p) = b_0 + \frac{m_0(p)}{1 + \frac{m_1(p)}{1 + \dots}} =: [b_0, [m_0(p), 1], [m_1(p), 1] \cdots [m_N(p), 1]] \quad (37)$$

where  $m_k(p)$  are monomials,  $m_k(p) = c_k p^{q_k}$ . Given a power series, the constants  $c_k$  and  $q_k$  are uniquely determined by requiring that the Maclaurin series of  $R_N$  coincides with the given series to the highest possible order allowed by the total degree of  $R_N$ . It follows that  $R_N(p)$  is in fact a way of rewriting a near-diagonal Padé approximant  $P_N(p)/Q_N(p)$ ,  $\deg(P_N) \approx \deg(Q_N)$ . This is an important representation of Padé approximants for a number of reasons, including the fact that the  $c_k$  are much smaller than the Padé coefficients, and that the  $c_k$  often have asymptotic expansions at large  $k$ , which give analytic information about the series. For Painlevé I we calculated  $R(p) = [0, [\frac{4p}{25}, 1], [\frac{49p^2}{75}, 1], \dots]$ , and observed empirically that, for large  $k$ ,  $m_k(p) \sim \frac{1}{4}p^2$ . A straightforward induction argument shows that the polynomials  $P_N$  and  $Q_N$  satisfy two-step recurrence relations [66], which can therefore be associated with orthogonal polynomials. Then the asymptotics of  $m_k(p)$  follows from Szegő asymptotics of orthogonal polynomials [67]. We

can then estimate the successive error as  $R_N - R_{N-1} \sim A(p)(z(p))^{2N}$ , for some  $A(p)$  independent of  $N$ , where the conformally mapped variable  $z(p)$  from (17) arises from solving the asymptotic recursion formulas. A deep result of Damanik and Simon characterizes the asymptotics  $m_k = p^2/4 + \epsilon_k$ , with  $\epsilon_k$  small enough [68]. This can be used to show that the accuracy in  $\mathbb{C}$  of a Padé-Borel approximant with  $N$  terms is  $O((1 - z^2(p))^{-1}z(p)^{2N})$ , roughly the same as that of the conformally mapped *Taylor series* in the unit disk. In particular, if  $|p| \geq 1$  and  $\Re p = 0$ , then  $|z(p)| = 1$ ; and thus standard Padé-Borel approximants diverge everywhere on the cuts. On the other hand, for small  $p$ ,  $z^2(p) \sim p^2/4$  meaning that, well inside the unit disk, Padé-Borel gives an  $O(4^{-N})$  accuracy improvement over the Taylor series. And, away from the cuts, for large  $p$  and  $N$ , a standard Borel-Padé approximation has accuracy  $O(pe^{-2N/|p|})$ , which translates to  $O(N^{3/4}|x|^{-5/4}e^{-\sqrt{8N}|x|})$  accuracy in the physical domain  $x$ . And the improvement of the conformally mapped Padé-Conformal-Borel transform in (20) over the Padé-Borel transform in (14) also scales like  $4^{-N}$ . Further details and applications will appear in [15].

*Resurgent Numerical Analysis:* our results suggest that it may also be fruitful to incorporate some ideas of resurgence into the sophisticated numerical analysis methods of [56, 57].

This material is based upon work supported by the U.S. Department of Energy, Office of Science, Office of High Energy Physics under Award Number DE-SC0010339 (GD), and by the National Science Foundation under Award Number DMS 1515755 (OC). Both authors thank the KITP at Santa Barbara for its hospitality during the Fall 2017 program “Resurgent Asymptotics in Physics and Mathematics” where much of this work was begun. Research at KITP is supported by the National Science Foundation under Grant No. NSF PHY-1125915. We thank A. Its, P. Nevai, and C. Bender for helpful discussions, comments and correspondence.

- 
- [1] C. N. Yang and T. D. Lee, “Statistical theory of equations of state and phase transitions. 1. Theory of condensation,” Phys. Rev. **87**, 404 (1952); T. D. Lee and C. N. Yang, “Statistical theory of equations of state and phase transitions. 2. Lattice gas and Ising model,” Phys. Rev. **87**, 410 (1952).
  - [2] M. E. Fisher, “The Nature of Critical Points”, pp. 1-159 in *Lectures in Theoretical Physics*, Vol. VII C, (Univ. of Colorado Press, 1965); M. E. Fisher, “Yang-Lee Edge Singularity and  $\phi^3$  Field Theory,” Phys. Rev. Lett. **40**, 1610 (1978).
  - [3] M. E. Fisher, “The theory of equilibrium critical phenomena”, Rep. Prog. Phys. **30**, 615 (1967).
  - [4] C. M. Bender and S. A. Orszag, *Advanced Mathematical Methods for Scientists and Engineers: Asymptotic Methods and Perturbation Theory*, (Springer, 1999).
  - [5] J. Zinn-Justin, *Quantum field theory and critical phenomena*, Int. Ser. Monogr. Phys. **113**, 1 (2002).
  - [6] H. Kleinert and V. Schulte-Frohlinde, *Critical properties of  $\phi^4$ -theories*, (World Scientific, 2001).
  - [7] E. Caliceti, M. Meyer-Hermann, P. Ribeca, A. Surzhykov and U. D. Jentschura, “From useful algorithms for slowly convergent series to physical predictions based on divergent perturbative expansions,” Phys. Rept. **446**, 1 (2007), arXiv:0707.1596.
  - [8] R. B. Dingle, *Asymptotic expansions: their derivation and interpretation*, (Academic Press, 1973).
  - [9] J. Ecalle, *Les fonctions resurgentes; Vols. 1-3*, (Pub. Math. d’Orsay, 1981-1985).
  - [10] O. Costin, *Asymptotics and Borel summability*, (Chapman and Hall/CRC, 2008).
  - [11] E. Delabaere, M. Loday-Richaud, C. Mitschi, D. Sauzin, *Divergent Series, Summability and Resurgence I-III*, (Lecture Notes in Mathematics, Volumes 2153-2155, Springer, 2017).
  - [12] I. Aniceto and R. Schiappa, “Nonperturbative Ambiguities and the Reality of Resurgent Transseries,” Commun. Math. Phys. **335**, no. 1, 183 (2015), arXiv:1308.1115.
  - [13] D. Dorigoni, “An Introduction to Resurgence, Trans-Series and Alien Calculus,” arXiv:1411.3585.
  - [14] I. Aniceto, G. Basar and R. Schiappa, “A Primer on Resurgent Transseries and Their Asymptotics,” arXiv:1802.10441.
  - [15] O. Costin and G. V. Dunne, to appear.
  - [16] P. A. Clarkson, “Painlevé equations - nonlinear special functions”, in *Orthogonal Polynomials and Special Functions: Computation and Application*, F. Márcellan and W. van Assche (Eds.), Lecture Notes in Mathematics, vol. **1883**, Springer-Verlag, Berlin (2006), pp 331-411.
  - [17] B. M. McCoy and T. T. Wu, *The Two Dimensional Ising Model* (Harvard Univ. Press, 1973).
  - [18] L. J. Mason and N. M. J. Woodhouse, *Integrability, Self-duality, and Twistor Theory* (London Mathematical Society Monographs, Oxford University Press, 1997).
  - [19] V. I. Gromak, I. Laine, S. Shimomura, *Painlevé Differential Equations in the Complex Plane*, (de Gruyter, 2002).
  - [20] A. S. Fokas, A. R. Its, A. A. Kapaev, V. Yu. Novokshenov, *Painlevé Transcendents: The Riemann-Hilbert Approach*, (American Mathematical Society, 2006).
  - [21] P. J. Forrester, *Log Gases and Random Matrices*, (Princeton University Press, Princeton, 2010).
  - [22] C. A. Tracy and H. Widom, “Painlevé Functions in Statistical Physics”, Publ. RIMS Kyoto Univ. **47**, 361-374 (2011).
  - [23] G. Bonelli, O. Lisovyy, K. Maruyoshi, A. Sciarappa and A. Tanzini, “On Painlevé/gauge theory correspondence,” Lett. Math. Phys. **107**, 2359 (2017), arXiv:1612.06235.
  - [24] A. S. Fokas, A. R. Its and A. V. Kitaev, “Discrete Painleve equations and their appearance in quantum gravity,” Commun. Math. Phys. **142**, 313 (1991); “The Isomonodromy approach to matrix models in 2-D quantum gravity,” Commun. Math. Phys. **147**, 395 (1992).

- [25] P. G. Silvestrov and A. S. Yelkhovsky, “Two-dimensional gravity as analytical continuation of the random matrix model,” *Phys. Lett. B* **251**, 525 (1990).
- [26] F. David, “Phases of the large  $N$  matrix model and nonperturbative effects in 2-d gravity,” *Nucl. Phys. B* **348**, 507 (1991); “Nonperturbative effects in matrix models and vacua of two-dimensional gravity,” *Phys. Lett. B* **302**, 403 (1993), arXiv:hep-th/9212106.
- [27] P. Di Francesco, P. H. Ginsparg and J. Zinn-Justin, “2-D Gravity and random matrices,” *Phys. Rept.* **254**, 1 (1995), arXiv:hep-th/9306153.
- [28] M. Mariño, “Nonperturbative effects and nonperturbative definitions in matrix models and topological strings,” *JHEP* **0812**, 114 (2008), arXiv:0805.3033.
- [29] O. Costin, “Exponential asymptotics, transseries, and generalized Borel summation for analytic rank one systems of ODE’s”, *Int. Math. Res. Notices*, **1995**, Issue 8, 377-417 (1995), arXiv:math/0608414.
- [30] O. Costin, “On Borel summation and Stokes phenomena of nonlinear differential systems”, *Duke Math. J.* **93**, No 2, 289-344 (1998), arXiv:math/0608408.
- [31] O. Costin and R. D. Costin, “On the formation of singularities of solutions of nonlinear differential systems in antistokes directions”, *Invent. Math.* **145**, 425-485 (2001).
- [32] O. Costin, R. D. Costin and M. Huang, “A direct method to find Stokes multipliers in closed form for P1 and more general integrable systems”, *Trans. Amer. Math. Soc.* **368**, 7579-7621 (2016).
- [33] P. Boutroux, “Recherches sur les transcendentes de M. Painlevé et l’étude asymptotique des équations différentielles du second ordre”, *Ann. École Norm.* **30**, 265-375 (1913); **31**, 99-159 (1914).
- [34] A. A. Kapaev and A. V. Kitaev, “Connection formulae for the first Painlevé transcendent in the complex domain”, *Lett. Math. Phys.* **27**, 243-252 (1993).
- [35] A. V. Kitaev, “Elliptic asymptotics of the first and the second Painlevé transcendents”, *Russian Math. Surveys* **49**, 81-150 (1994).
- [36] N. Joshi and A. V. Kitaev, “On Boutroux’s *Tritronquée* Solutions of the First Painlevé Equation”, *Stud. Appl. Math.* **107**, 253-291 (2001).
- [37] Y. Takei, “On the connection formula for the first Painlevé equation”, *RIMS Kôkyûroku*, **931**, 70-99 (1995).
- [38] B. Dubrovin, T. Grava, and C. Klein, “On universality of critical behavior in the focusing nonlinear Schrödinger equation, elliptic umbilic catastrophe and the tritronquée solution to the Painlevé-I equation”, *J. Nonlinear Sci.* **19**, 57-94 (2009).
- [39] V. Yu. Novokshenov, “Padé Approximations for Painlevé I and II Transcendents”, *Theor. Math. Phys.* **159**(3), 853-862 (2009).
- [40] S. Garoufalidis, A. Its, A. Kapaev and M. Mariño, “Asymptotics of the instantons of Painlevé I,” *Int. Math. Res. Not.* **2012**, no. 3, 561 (2012), arXiv:1002.3634.
- [41] I. Aniceto, R. Schiappa and M. Vonk, “The Resurgence of Instantons in String Theory,” *Commun. Num. Theor. Phys.* **6**, 339 (2012), arXiv:1106.5922.
- [42] O. Costin, M. Huang, S. Tanveer, “Proof of the Dubrovin conjecture and analysis of the tritronquée solutions of PI”, *Duke Math. J.* **163**, no. 4, 665-704 (2014), arXiv:1209.1009.
- [43] K. Iwaki and A. Saenz, “Quantum Curve and the First Painleve Equation,” *SIGMA* **12**, 011 (2016) arXiv:1507.06557; K. Iwaki, “2-parameter  $\tau$ -function for the first Painlevé equation -Topological recursion and direct monodromy problem via exact WKB analysis,” arXiv:1902.06439.
- [44] O. Lisovyy and J. Roussillon, “On the connection problem for Painlevé I,” *J. Phys. A* **50**, no. 25, 255202 (2017), arXiv:1612.08382.
- [45] E. L. Ince, *Ordinary Differential Equations*, (Dover, 1956).
- [46] P. A. Clarkson (Ed.), *Painlevé Transcendents*, NIST Digital Library of Mathematical Functions, <https://dlmf.nist.gov/32>.
- [47] M. V. Berry and C. J. Howls, “Hyperasymptotics for integrals with saddles”, *Proc. R. Soc. A* **434**, 657 (1991).
- [48] S. Graffi, V. Grecchi and B. Simon, “Borel summability: Application to the anharmonic oscillator,” *Phys. Lett.* **32B**, 631 (1970).
- [49] G. A. Baker and P. Graves-Morris, *Padé Approximants*, (Cambridge University Press, 1996).
- [50] C. Brezinski, “Extrapolation algorithms and Pade approximations”, *App. Numer. Math.* **20** (3): 299-318 (1996).
- [51] P. Henrici, *Applied and Computational Complex Analysis*, Vol. 2 (Wiley, 1977).
- [52] D. S. Gaunt and A. J. Guttmann, “Asymptotic Analysis of Coefficients”, in *Phase Transitions and Critical Phenomena, Vol. 3: Series Expansions for Lattice Models*, C. Domb and M. S. Green (Eds) (Academic Press, 1974).
- [53] G. ’t Hooft, “Can We Make Sense Out of Quantum Chromodynamics?,” *Subnucl. Ser.* **15**, 943 (1979).
- [54] D. I. Kazakov, D. V. Shirkov and O. V. Tarasov, “Analytical Continuation of Perturbative Results of the  $g\phi^4$  Model Into the Region  $g$  Is Greater Than or Equal to 1,” *Theor. Math. Phys.* **38**, 9 (1979) [*Teor. Mat. Fiz.* **38**, 15 (1979)].
- [55] P. Gonnet, S. Güttel, L. N. Trefethen, “Robust Padé Approximation via SVD”, *SIAM Rev.* **55**, 101-117 (2013).
- [56] F. Bornemann, “On the Numerical Evaluation of Distributions in Random Matrix Theory: A Review”, *Markov Proc. Relat. Fields* **16**, 803-866 (2010), arXiv:0904.1581.
- [57] B. Fornberg and J. A. C. Weideman, “A numerical methodology for the Painlevé equations”, *J. Comp. Phys.* **230**, 5957-5973 (2011).
- [58] D. Masoero, “Poles of Integrale Tritronquee and Anharmonic Oscillators. Asymptotic localization from WKB analysis,” *Nonlinearity* **23**, 2501 (2010), arXiv:1002.1042; “Poles of Integrale Tritronquee and Anharmonic Oscillators. A WKB Approach”, *J. Phys. A: Math. Theor.* **43** 095201 (2010), arXiv:0909.5537.
- [59] C. M. Bender and J. Komijani, “Painlevé Transcendents and PT-Symmetric Hamiltonians,” *J. Phys. A* **48**, no. 47, 475202

- (2015), arXiv:1502.04089.
- [60] V. Yu. Novokshenov, “Poles of Tritronquée Solution to the Painlevé I Equation and Cubic Anharmonic Oscillator”, Reg. Chaotic Dyn. **15**, 390 - 403 (2010).
  - [61] V. Yu. Novokshenov, “Movable poles of the solutions of Painlevé’s equation of the third kind and their relation with Mathieu functions”, Func. Anal. Appl. **20**, 113 (1986) [Funk. Anal. Pril. **20**, 38 (1986)].
  - [62] S. L. Lukyanov, “Critical values of the Yang-Yang functional in the quantum sine-Gordon model,” Nucl. Phys. B **853**, 475 (2011), arXiv:1105.2836.
  - [63] A. Gorsky, A. Milekhin and N. Sopenko, “Bands and gaps in Nekrasov partition function,” JHEP **1801**, 133 (2018), arXiv:1712.02936.
  - [64] A. Litvinov, S. Lukyanov, N. Nekrasov and A. Zamolodchikov, “Classical Conformal Blocks and Painleve VI,” JHEP **1407**, 144 (2014), arXiv:1309.4700.
  - [65] G. V. Dunne, “Resurgence, Painleve Equations and Conformal Blocks,” arXiv:1901.02076.
  - [66] H. S. Wall, *Analytic Theory of Continued Fractions*, (American Mathematical Society, 1948).
  - [67] G. Szegő, *Orthogonal Polynomials*, (American Math Society, 1939).
  - [68] D. Damanik and B. Simon, “Jost functions and Jost solutions for Jacobi matrices, I. A necessary and sufficient condition for Szegő asymptotics”, Invent. Math. **165**, 1-50 (2006).